Low Vacuum Annealing of Cellulose Acetate on Nickel Towards Transparent Conductive CNT−Graphene Hybrid Films

Duc Dung Nguyen,*,[†] Rajanish N. Tiwari,[†] Yuki Matsuoka,[†] Goh Hashimoto,[‡] Eiji Rokuta,[‡] Yu-Ze Chen,[§] Yu-Lun Chueh,[§] and Masamichi Yoshimura[†]

[†]Toyota Technological Institute, 2-12-1 Hisakata, Tempaku, Nagoya 468-8511, Japan
[‡]Faculty of Science and Engineering, Meijo University, 1-501 Shiogamaguchi, Tempaku, Nagoya 468-8502, Japan
[§]Department of Materials Science & Engineering, National Tsing-Hua University, Hsinchu 30013, Taiwan

S Supporting Information

ABSTRACT: We report a versatile method based on low vacuum annealing of cellulose acetate on nickel (Ni) surface for rapid fabrication of graphene and carbon nanotube (CNT)−graphene hybrid films with tunable properties. Uniform films mainly composed of tri-layer graphene can be achieved via a surface precipitation of dissociated carbon at 800 °C for 30 seconds under vacuum conditions of ∼0.6 Pa. The surface precipitation process is further found to be efficient for joining the precipitated graphene with pre-coated CNTs on the Ni surface, consequently, generating the hybrid films. As expected, the hybrid films exhibit substantial opto-electrical and field electron emission properties superior to their individual counterparts. The finding suggests a promising route to hybridize the graphene with diverse nanomaterials for constructing novel hybrid materials with improved performances.

KEYWORDS: graphene, carbon nanotubes, transparent conducting films, surface precipitation, low vacuum annealing, CNT−graphene hybrid films
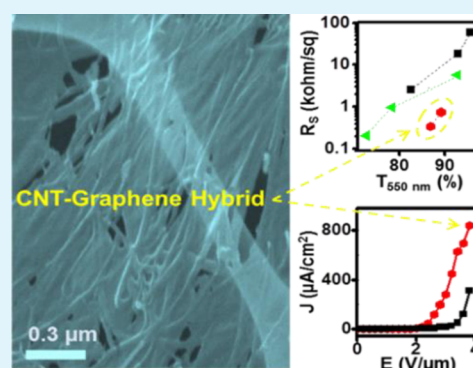
INTRODUCTION

As the representatives of low dimensional carbon allotropes, carbon nanotubes (CNTs)[1] and graphene[2] have attracted great attention owing to their intriguing properties.[3−8] Recent studies indicate that hybrid materials of CNTs and graphene exhibit considerably improved electrical, thermal, mechanical, and electrochemical properties compared to each of single components.[9−16] Up to date, the preparation of CNTs is becoming mature while graphene fabrication is still being developed. In general, graphene oxide (GO) is preferably selected for hybridization with CNTs because it is beneficial for mass production at low cost.[9−11,14,15] However, restoration of graphitic network within GO requires high temperature (1000 °C) treatment[10,14] or enormously toxic chemical such as hydrazine;[9,11,15] thus, special care is required when handling. Consequently, graphene grown by chemical vapor deposition (CVD) methods[17,18] is obviously preferred for incorporation with CNTs; nevertheless, long processing time and high growth temperature may limit its practical use at industrial scale. In this regard, modified CVD methods have been recently proposed to reduce processing time and/or lower growth temperature in combination with reduction of electric power by direct heating the catalytic substrates.[19,20] Therefore, it is highly imperative to develop alternative graphene fabrication methods, which are time- and power-saving, environmentally friendly, and

especially compatible with processing of CNT−graphene hybrids.

Early hybridization methods are layer by layer assembly of CNTs and reduced GO sheets via electrostatic interactions,[10] wet blending of CNTs and GO sheets,[9,11,15,16] or solid-phase layer stacking CNT networks on a graphene film.[12] Most recently, partially unzipping/splitting of CNTs via metal-assisted thermal etching[21] and potassium vapor intercalation followed by solvent quenching[22] have been demonstrated as efficient routes for preparation of CNT−graphene hybrids. In this study, we present a new strategy based on a rapid carbon precipitation on nickel (Ni) surfaces under low vacuum conditions to fabricate not only graphene but also CNT−graphene hybrid films. Our fabrication/hybridization method has advantages of short time processing, low power consumption, and avoidance of explosive gases and toxic chemicals. Cellulose acetate (CA) is used as a solid carbon precursor for the precipitation of graphene on Ni surfaces while a CNT network coated on a Ni surface serves as a host component for joining with the precipitated graphene, i.e., producing CNT−graphene hybrid films. As expected, the hybrid films reveal considerable opto-electrical and field
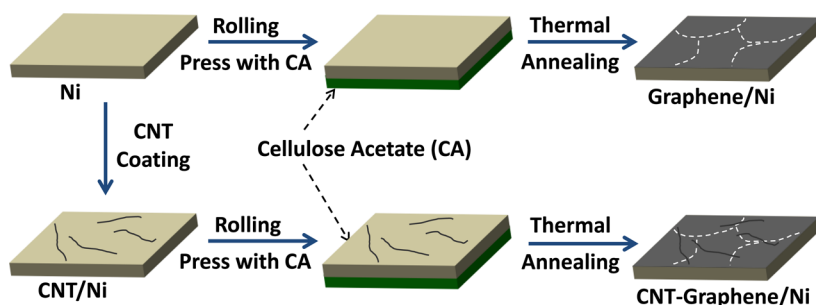
Figure 1. Illustration for the fabrication of graphene and CNT−graphene hybrid films.
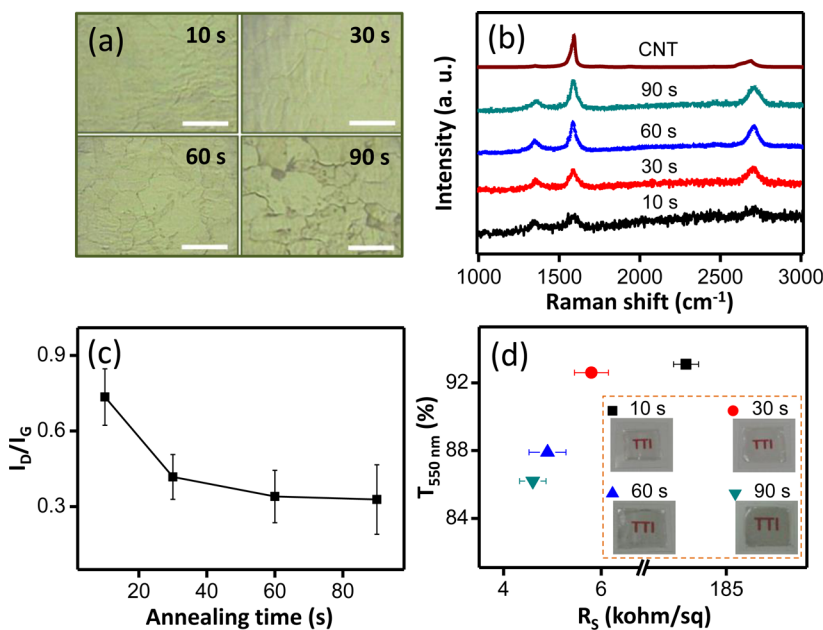

Figure 2. Typical OM images (a), Raman spectra (b), and I_D/I_G ratios (c) of as-fabricated graphene films processed at different annealing times. R_S versus T_{550} of the transferred graphene films (d); insets are photographs of the films, demonstrating the optical transparency. Scale bars in part a are 20 μm. A Raman spectrum of the CNTs in part b is for reference only.

electron emission properties superior to their individual counterparts. These findings suggest a versatile route for development of graphene-based hybrid materials and potential applications where tunable opto-electrical and field emission properties are desired.

■ EXPERIMENTAL SECTION

Fabrication of Graphene and CNT−Graphene Hybrid Films. Ni foil (Nilaco) with thickness of 10 μm and CA membrane (Whatman) were used as a catalytic substrate and a solid carbon precursor for fabrication of graphene. At first, the Ni was ultrasonically cleaned in an acetone bath for 10 min to remove contaminants resided on its surfaces. Subsequently, the CA membrane was mechanically pressed on a Ni surface utilizing a roller. The sample was then placed in a quartz container inside a lamp annealing system (Mila 5000, Ulvac). At a base vacuum level of ~0.6 Pa, the sample was heated to desired temperatures with a heating rate of ~3.0 °C s^{-1}. Graphene films with different graphitic qualities could be obtained by varying the annealing times and temperatures. The cooling rates from annealing temperatures to 500 °C are of 13−15 °C s^{-1}. Hybrid films of CNTs and graphene were produced using the optimized conditions for fabrication of graphene with a modification that the Ni substrates coated with CNT networks were employed instead.

Sample Characterizations. Formation of graphene films and their graphitic quality were characterized using optical microscope (OM) and Raman spectroscope (Renishaw) with a 532 nm laser. An

atomic force microscope (AFM, Bruker) was operated in peak force tapping mode to verify the thickness of the graphene. The structures of graphene and CNT−graphene hybrid were examined using high resolution transmission electron microscopes (HRTEM, JEOL JEM-2100). Morphology of CNT networks, graphene, and CNT−graphene films were observed utilizing a field emission scanning electron microscope (FESEM, Hitachi 4700). The sheet resistance and optical transmittance spectra were measured using a two probe method and a UV−Vis−NIR spectrophotometer (V630, Jasco), respectively. A typical parallel plate configuration was employed for field electron emission measurement at a vacuum level of ~2.6 × 10^{-6} Pa. A CNT network (sheet resistance of 0.86 kohm/sq and transmittance of 62.4%), and its corresponding hybrid film on Ni were employed as cathodes, respectively. An indium tin oxide coated glass was used as the anode and separated from the CNT or CNT−graphene based cathodes by a 100 μm thick spacer.

■ RESULTS AND DISCUSSION

Carbon precipitation as single-layer and multi-layer graphene on the surface of bulk transition metals is extensively proposed.[23,24] This phenomenon is attributed to the intensive temperature-dependence of carbon solubility in transition metals. Using the concept, graphene films have been recently fabricated by thermal annealing under ultra-high/high vacuum conditions[25,26] and CVD.[17,27,28] Herein, a near-infrared lamp annealing system was employed for fabrication of graphene and
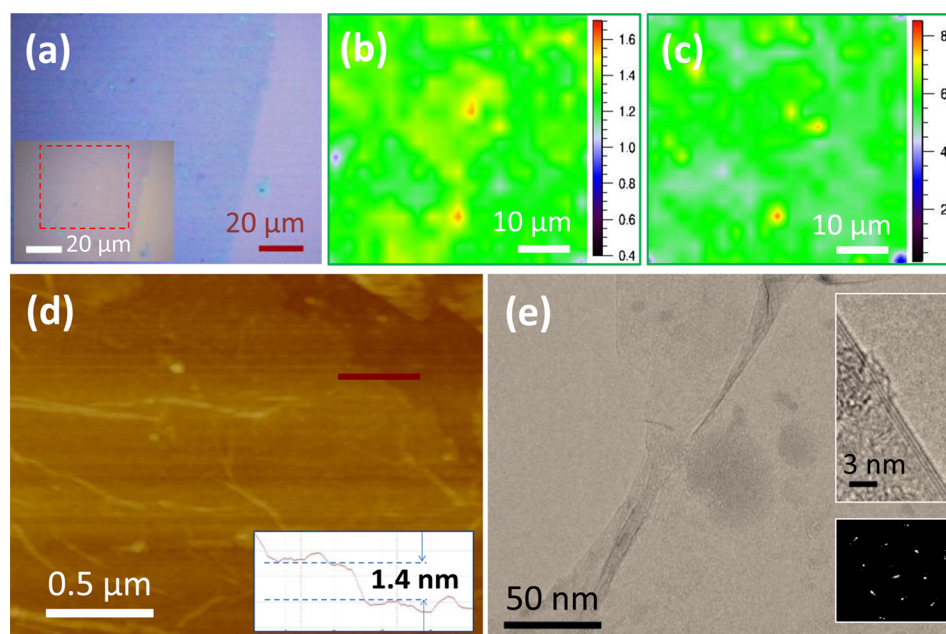
Figure 3. Typical OM image of the transferred graphene film on SiO_2/Si, inset is its higher magnified image (a). Raman mapping of I_G/I_{2D} ratio (b) and FWHM (c) of 2D peak. A typical AFM image with a line profile (d) and a TEM image (e) of the graphene. (e) Top inset is a tri-layered structure; the bottom inset is an electron diffraction pattern of the graphene.

CNT–graphene hybrid films under low vacuum conditions, respectively. Figure 1 illustrates the procedure for the fabrication processes. Briefly, a cleaned Ni substrate is first coated with either a CA membrane or a CNT network followed by the CA membrane on the opposite side. Subsequently, the sample is loaded into a chamber, which is then evacuated and rapidly heated to a desired temperature. At elevated temperatures, carbon atoms dissociated from the CA diffuse into the Ni followed by the surface precipitation to form graphene on both sides of the Ni substrate or CNT–graphene hybrid on the CNT-coated side and graphene on the CNT-free side of the Ni substrate.

In order to achieve graphene films with uniform thickness and good graphitic quality, several critical parameters need to be optimized. We first studied the effect of annealing time on the formation, uniformity, and crystalline quality of as-fabricated films.

Figure 2a shows OM images of CA coated Ni substrates after annealing at 800 °C for varied times. Uniform color is observed at the samples annealed for 10 and 30 seconds, indicating relatively homogeneous films. As the annealing time increased to 60 and 90 seconds, dark flakes are clearly seen nearby the grain boundaries. Noticeably, surface coverage by such dark regions increases as the annealing time increases. To comprehend this time evolution of the as-fabricated films, Raman spectroscopy was employed to probe on the plane regions of grains and the flakes (see Figure 2a), respectively. All samples exhibit the Raman fingerprints for graphene/graphite, identified as three prominent peaks, including the D peak at ~1351 cm^{-1}, associated with disordered sp^3-hybridized carbon as found in defects or impurities in carbon materials; the G peak at ~1583 cm^{-1}, which results from the E_{2g} vibrational mode of sp^2 bonded carbon; and the 2D peak at ~2703 cm^{-1}, which is the second-order vibration caused by the scattering of phonons at the zone boundary.[29,30] The dark flakes existed in the samples annealed for 60 and 90 seconds are attributed to multilayer graphene/graphite according to the criterion of large

intensity ratios of I_G/I_{2D}[27,29−31] as seen in Supporting Information Figure S1a. Raman spectra acquired from the plane regions of grains reveal that G peak possesses intensity comparable to that of the 2D peak in each sample, as shown in Figure 2b. These spectra exhibit profile features of tri-layer and/or bi-layer graphene.[17,27,31−34] A typical Raman spectrum of the CNTs (Aldrich-637351) was included in Figure 2b as a reference for the difference between tubular and planar graphitic structures. In order to evaluate graphitic quality of the graphene films processed at different annealing times, the intensity ratios of I_D/I_G were extracted from their spectra (acquired on the plane regions of grains) for comparison. As shown in Figure 2c, the I_D/I_G ratio decreases slightly when annealing time increases, implying that longer annealing time results in better graphitic quality.

Nevertheless, this hastens the formation and expansion of the graphitic flakes (Figure 2a), which are probably detrimental to the opto-electrical performance of the graphene films. The occurrence of such flakes involves Ni grain boundaries, which are recognized as preferential sites for carbon accumulation.[35,36] Once a specific nucleation site is activated, it quickly "pumps out" carbon atoms, leading to the lateral growth of multilayer graphene/graphite flakes surrounding the grains, as demonstrated in Supporting Information Figure S1b. On the other hand, bi- or tri-layer graphene was predominantly formed on the plane regions of grains via carbon precipitation and crystallization either during annealing or cooling.

For evaluation of opto-electrical performance in terms of annealing time, the graphene films were transferred onto transparent polymer substrates. Figure 2d indicates the sheet resistance (R_S) versus transmittance at wavelength of 550 nm (T_{550}) of the transferred graphene films processed at different annealing times. Insets in Figure 2d are photographs of the corresponding graphene films, demonstrating their optical transparent property. There is no substantial difference in R_S but a grave decrease in T_{550} is observed as the annealing time increases from 30 to 90 seconds. This indicates that the
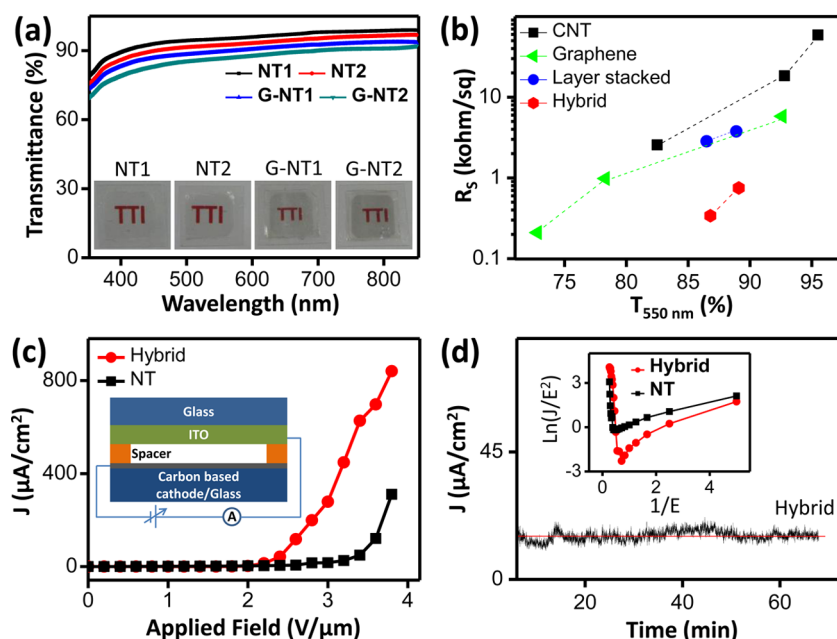
Figure 4. Optical transmittance spectra of the CNT and CNT−graphene hybrid films (a). Insets are photographs of the corresponding films. R_S versus T_{550} for the CNT, graphene, layer stacked, and hybrid films (b). Field emission current density versus applied field (J−E) of the CNT and hybrid films (c), inset is a typical configuration for field emission measurement. Current stability of the hybrid film (d), inset is F−N plots for the CNT and hybrid films.

presence of multilayer graphene/graphite flakes has a negligible contribution to the electrical conductivity but reasonably reduces the optical transparency of the graphene films. As the annealing time decreases to 10 seconds, optical transparency of the film is high but much larger R_S attained. This can be ascribed for different graphitic qualities as revealed by aforementioned Raman data in which the I_D/I_G ratio of the 10 second-obtained film is highest, that is, the most defective graphene film. Moreover, the moderately broad peak in the range 1250−1660 cm^{-1} is indicative of a film composed of graphene and amorphous carbon. This implies that a partial amount of the precipitated carbon atoms could be crystallized in such a short time, but not enough for reaching a regime with good graphitic quality. Thus, annealing for 30 seconds is inferred as the optimized time among others.

Additionally, the effect of annealing temperature on the formation of graphene films was investigated while keeping the annealing time fixed at 30 seconds. Raman data approve that few/multi-layer graphene films were obtained as the annealing temperature increased to 850 and 900 °C (Supporting Information Figure S2). Although R_S of these films could remarkably reduce to ∼0.98−0.21 kohm/sq, their optical transmittance of ∼81−72% is probably incompatible for highly transparent electronic applications. Contrarily, lower annealing temperatures lead to the films of highly defective graphene blended with amorphous carbon (750 °C) or amorphous carbon (700 °C), as evidenced by Raman data (Supporting Information Figure S2). Therefore, we chose 800 °C and 30 seconds as the parameters for the carbon precipitation process.

For further characterizations, the graphene fabricated using the carbon precipitation was transferred on a SiO$_2$/Si substrate using a wet etching method with poly(methyl methacrylate) (PMMA) as a supportive scaffold and a diluted HNO$_3$ and acetone for Ni etching and PMMA dissolving agents, respectively. Figure 3a is an OM image of the transferred graphene; inset is its higher magnification. Raman mapping

analyses were performed on the square marked area as indicated in the inset of Figure 3a.

Figure 3b shows a Raman map of the G to 2D peak intensity with the uniformly distributed green color (I_G/I_{2D} ratios of 1.2−1.5) covering more than 90% of the recorded area. The full width at half maximum (FWHM) of the 2D peak were also mapped in colors (Figure 3c), which were arithmetically valued in the range of 45−75 cm^{-1}. It is revealed that higher I_G/I_{2D} ratios are consistent with larger FWHM when comparing the two maps shown in Figure 3b and c. Considering to different synthetic conditions, a tri-layer graphene is deduced to possess the I_G/I_{2D} ratio of 1.0−2.6 and FWHM of 50−70 cm^{-1}; the inferred values for bi-layer are of 0.7−1.3 and 45−60 cm^{-1}, respectively.[17,27,32−34] Using these criteria, the film is thus estimated to be mainly composed of tri-layer graphene and the rest are bi-layer and few-layer graphene. Figure 3d shows a typical AFM image with uniform color contrast, that is, uniform thickness, although ripple structures were formed either due to the difference between the thermal expansion coefficients of Ni and graphene or during the transfer process. Inset in Figure 3d is a line profile indicating the graphene thickness is ∼1.4 nm, suggestive of a tri-layer graphene.[17] TEM examination further confirms the graphitic structure and the number of graphene layers. Figure 3e is a low magnification TEM image of the graphene with sheet-like and folded structure. The electron diffraction pattern shown as the bottom inset of Figure 3e reveals the typical hexagonal crystalline structure of the graphene. An imaged graphene edge at high magnification (top inset of Figure 3e) shows three carbon layers, verifying the tri-layer nature of the graphene film.

Remarkably, the carbon precipitation process was found to be effective in fabricating CNT−graphene hybrid films with improved properties. This can be elucidated that during annealing and/or cooling, the precipitated carbon atoms are crystallized to form graphene on CNT-free areas of the Ni surface. Simultaneously, such atoms precipitating under or

nearby CNTs are preferentially filled into defective sites of the CNTs, creating C−C links between CNTs and the adjacent precipitated graphene, that is, constructing the CNT−graphene hybrids. The formation, morphology, and structure of the hybrid films were examined using FESEM, TEM, and Raman spectroscopy (Figure S3−S5 and discussion in Supporting Information). To demonstrate advantages of the hybrid films in terms of potential applications, their opto-electrical properties were compared. Figure 4a shows optical transmittance spectra as a function of wavelength of two CNT networks with different densities (assigned as NT1, NT2) and their corresponding hybrid films (assigned as NT1-G and NT2-G); insets are their photographs, which indicate the optical transparency. By comparing the spectra, optical transparency of the hybrid films can be deduced to be equal to the product of their individual optical transparencies, that is, $T_{Hybrid} = T_{CNT} \times T_{Graphene}$. Therefore, a hybrid film with desired transparency can be manipulated by selecting CNT networks with controlled optical properties, that is, controlling CNT density. The advantages associated with the hybridization is illustrated in Figure 4b, indicating data for R_S versus T_{550} of the graphene films fabricated at different temperatures (one was repeated for comparison), CNT networks, the hybrid films (NT1-G and NT2-G), and layer stacked CNT/graphene films. Preparation of the layer stacked films was carried out by coating either NT1 or NT2 network on the graphene/Ni followed by a transfer process (adopting the coating and transferring methods described in Supporting Information). By comparison, CNT and graphene films reveal analogous $R_S \sim 1.0-18.4$ kohm/sq with corresponding T_{550} in the range ~79−93%. These values are close to the entry level (1.0 kohm/sq@80%T_{550}) at which the materials become valuable for some transparent conductor applications[37] and are comparable to those of graphene films fabricated using energy- and time-saving procedures.[19,38] As the CNT networks ($R_S = 59.0-18.4$ kohm/sq; $T_{550} = 95.5-92.8\%$) were incorporated with the graphene film, their R_S significantly reduced to 3.76−2.84 kohm/sq for the layer stacked films and 0.75−0.34 kohm/sq for the hybrid films while their transparencies were maintained in the range 89.1−86.5%. The values are comparable to those of the solid-phase layer stacked films where the graphene was grown by CVD at temperature of 1000 °C ($R_S = 0.73-0.40$ kohm/sq, $T_{550} = 90.0-70.0\%$).[12]

These values are superior than those of hybrid films processed via plasma enhanced CVD ($R_S = 9.0-6.0$ kohm/sq, $T_{550} = 85.0-80.0\%$),[39] the layer by layer self-assembled hybrid films annealed at 1000 °C in a hydrogen environment ($R_S = 30.0-8.0$ kohm/sq, $T_{550} = 90.0-81.0\%$),[10] and the wet-blended hybrid films prepared using anhydrous hydrazine as a solvent ($R_S = 0.48-0.33$ kohm/sq, $T_{550} = 73.3-65.8\%$).[11] The enhancement observed in the layer stacked films is attributed to the extension of conjugated network by the two carbon allotropes.[12] The supreme opto-electrical performance achieved from the hybrid films is possibly owing to the formation of the C−C links between CNTs and graphene at the moderate temperature. These links prohibit CNTs and graphene domains from sliding within the films, leading to a substantial decrease of the overall resistance.[39−42] Moreover, defects of the CNTs could be effectively healed during the hybridization by the precipitated and crystallized carbon atoms, which filled defective sites and restored the six-membered aromatic rings. It is worth to note that via the rapid hybridization with the graphene, R_S of the CNT networks intensely decrease two orders of magnitude without severe change in optical

transparency. By selecting higher conductive CNT networks and/or other applicable nano-materials in combination with post treatments, superior opto-electrical performances are anticipated for resultant films.

Furthermore, the precipitated graphene in the hybrid film could serve as an interfacial layer for reducing contact resistance between the CNTs and Ni substrate, resulting in improved field electron emission performance. Figure 4c shows the dependence of field emission current density on the applied electric field (J−E) for the CNT and its hybrid films; the inset is the parallel plate configuration for field emission measurement. The measured current was observed to obey the Fowler−Nordheim law where the current density is related to applied electric field as $J = (A\beta^2 E^2/\Phi)\exp(-B\Phi^{3/2}/\beta E)$, where J is the current density in A/m^2, E is the electric field in V/m, Φ is the work function in eV, β is the field enhancement factor at sharp geometry, $A = 1.54 \times 10^{-6}$ A·eV·V^{-2} and $B = 6.83 \times 10^9$ eV$^{-3/2}$·V·m^{-1}.[43] The turn-on electric field (E_{to}) defined as the magnitude of the applied electric field at a current density of 10 μA/cm^2 of the CNT and hybrid films are 2.68 and 2.12 V/μm, respectively. This value is lower than that of CNTs on graphite film ($E_{to} = \sim 5$ V/μm)[44] and comparable to those of CNTs/graphene hybrid films[45] ($E_{to} = 1.30-2.84$ V/μm) and vertically aligned CNTs on graphene[46] ($E_{to} = 0.98-2.35$ V/μm). The lower E_{to} observed in the hybrid film can be attributed to the presence of the graphene interfacial layer, which has strongly physicochemical interaction with the Ni.[47] These facilitate electron transport from Ni through graphene to CNTs, consequently enhancing field emission properties. As shown in Figure 4d, the emission current versus time of the hybrid film was found to be stable for duration of time. Inset of Figure 4d reveals the linear Fowler−Nordheim behavior, indicating a true field emission signature from CNTs and its hybrid film.

■ CONCLUSIONS

In summary, we have developed a versatile and environmentally friendly method to fabricate graphene films mainly composed of tri-layer graphene on the Ni under low vacuum conditions by rapid thermal annealing. Significantly, the fabrication process was found to be effective for simultaneously joining the as-precipitated graphene with pre-coated CNTs on the Ni surface, consequently establishing a new type of hybrid films. The hybrid films reveal substantially improved opto-electrical and field electron emission performances compared to each of their individual counterparts. Using the hybridization concept presented herein, we strongly believe that a variety of nano-materials with fascinating properties can be hybridized with the transparent and conductive graphene for constructing new hybrid materials with enhanced properties.

■ ASSOCIATED CONTENT

ⓈSupporting Information

Preparation of CNT networks on the Ni surface, transfer of graphene, and its hybrid films onto polymer substrates, Raman spectra, FESEM images, TEM images, and discussion on the formation of the CNT−graphene hybrid films. This material is available free of charge via the Internet at http://pubs.acs.org.

■ AUTHOR INFORMATION

Corresponding Author
*Fax: +81-52-809-1851. Phone: +81-52-809-1852. Email: ddnguyen@toyota-ti.ac.jp, ddnguyen161@gmail.com.

Author Contributions

The manuscript was written through contributions of all authors. All authors have given approval to the final version of the manuscript.

Notes

The authors declare no competing financial interest.

■ REFERENCES

(1) Iijima, S. Helical Microtubules of Graphitic Carbon. *Nature* **1991**, *354*, 56−58.

(2) Novoselov, K. S.; Geim, A. K.; Morozov, S. V.; Jiang, D.; Zhang, Y.; Dubonos, S. V.; Grigorieva, I. V.; Firsov, A. A. Electric Field Effect in Atomically Thin Carbon Films. *Science* **2004**, *306*, 666−669.

(3) Kaiser, A. B.; Skákalová, V. Electronic Conduction in Polymers, Carbon Nanotubes and Graphene. *Chem. Soc. Rev.* **2011**, *40*, 3786−3801.

(4) Ha, S. H.; Jeong, Y. S.; Lee, Y. J. Free Standing Reduced Graphene Oxide Film Cathodes for Lithium Ion Batteries. *ACS Appl. Mater. Interfaces* **2013**, *5*, 12295−12303.

(5) Kim, D.; Han, J. Y.; Lee, D.; Lee, D.; Jeon, D. Y. Facile Conversion of a Cellulose Acetate Laminate Film to Graphene by a Lamination Process and Post-Annealing. *J. Mater. Chem.* **2012**, *22*, 20026−20031.

(6) Deng, L.; Eichhorn, S. J.; Kao, C.-C.; Young, R. J. The Effective Young's Modulus of Carbon Nanotubes in Composites. *ACS Appl. Mater. Interfaces* **2011**, *3*, 433−440.

(7) Nguyen, D. D.; Tai, N.-H.; Lee, S.-B.; Kuo, W.-S. Super-hydrophobic and Superoleophilic Properties of Graphene-based Sponges Fabricated Using a Facile Dip Coating Method. *Energy Environ. Sci.* **2012**, *5*, 7908−7912.

(8) Liao, R.; Tang, Z.; Lin, T.; Guo, B. Scalable and Versatile Graphene Functionalized with the Mannich Condensate. *ACS Appl. Mater. Interfaces* **2013**, *5*, 2174−2181.

(9) Tung, V. C.; Chen, L. M.; Allen, M. J.; Wassei, J. K.; Nelson, K.; Kaner, R. B.; Yang, Y. Low-Temperature Solution Processing of Graphene−Carbon Nanotube Hybrid Materials for High-Performance Transparent Conductors. *Nano Lett.* **2009**, *9*, 1949−1955.

(10) Hong, T. K.; Lee, D. W.; Choi, H. J.; Shin, H. S.; Kim, B. S. Transparent, Flexible Conducting Hybrid Multilayer Thin Films of Multiwalled Carbon Nanotubes with Graphene Nanosheets. *ACS Nano* **2010**, *4*, 3861−3868.

(11) Huang, J. H.; Fang, J.-H.; Liu, C.-C.; Chu, C.-W. Effective Work Function Modulation of Graphene/Carbon Nanotube Composite Films As Transparent Cathodes for Organic Optoelectronics. *ACS Nano* **2011**, *5*, 6262−6271.

(12) Li, C. Y.; Li, Z.; Zhu, H. W.; Wang, K. L.; Wei, J. Q.; Li, X.; Sun, P.; Zhang, H.; Wu, D. Graphene Nano-"patches" on a Carbon Nanotube Network for Highly Transparent/Conductive Thin Film Applications. *J. Phys. Chem. C* **2010**, *114*, 14008−14012.

(13) Yu, A. P.; Ramesh, P.; Sun, X. B.; Bekyarova, E.; Itkis, M. E.; Haddon, R. C. Enhanced Thermal Conductivity in a Hybrid Graphite Nanoplatelet-Carbon Nanotube Filler for Epoxy Composites. *Adv. Mater.* **2008**, *20*, 4740−4744.

(14) Chen, M.; Tao, T.; Zhang, L.; Gao, W.; Li, C. Highly Conductive and Stretchable Polymer Composites Based on Graphene/MWCNT Network. *Chem. Commun.* **2013**, *49*, 1612−1614.

(15) Cheng, Y. W.; Lu, S. T.; Zhang, H. B.; Varanasi, V.; Liu, J. Synergistic Effects from Graphene and Carbon Nanotubes Enable Flexible and Robust Electrodes for High-Performance Supercapacitors. *Nano Lett.* **2012**, *12*, 4206−4211.

(16) Chen, P.; Xiao, T. Y.; Qian, Y. H.; Li, S. S.; Yu, S. H. A Nitrogen-Doped Graphene/Carbon Nanotube Nanocomposite with Synergistically Enhanced Electrochemical Activity. *Adv. Mater.* **2013**, *25*, 3192−3196.

(17) Reina, A.; Jia, X. T.; Ho, J.; Nezich, D.; Son, H. B.; Bulovic, V.; Dresselhaus, M. S.; Kong, J. Large Area, Few-Layer Graphene Films on Arbitrary Substrates by Chemical Vapor Deposition. *Nano Lett.* **2009**, *9*, 30−35.

(18) Bae, S. K.; Kim, H. K.; Lee, L.; Xu, X.; Park, J. S.; Zheng, Y.; Balakrishnan, J.; Lei, T.; Kim, H. R.; Song, Y. I. Roll-to-Roll Production of 30-inch Graphene Films for Transparent Electrodes. *Nat. Nanotechnol.* **2010**, *5*, 574−578.

(19) Yamada, T.; Ishihara, M.; Kim, J.; Hasegawa, M.; Iijima, S. A Roll-to-Roll Microwave Plasma Chemical Vapor Deposition Process for the Production of 294 mm Width Graphene Films at Low Temperature. *Carbon* **2012**, *50*, 2615−2619.

(20) Piner, R.; Li, H.; Kong, X.; Tao, L.; Kholmanov, I. N.; Ji, H.; Lee, W. H.; Suk, J. W.; Ye, J.; Hao, Y.; Chen, S.; Magnuson, C. W.; Ismach, A. F.; Akinwande, D.; Ruoff, R. S. Graphene Synthesis via Magnetic Inductive Heating of Copper Substrates. *ACS Nano* **2013**, *7*, 7495−7499.

(21) Yu, F.; Zhou, H.; Zhang, Z.; Wang, G.; Yang, H.; Chen, M.; Tao, L.; Tang, D.; He, J.; Sun, L. Controlled Fabrication of Intermolecular Junctions of Single-Walled Carbon Nanotube/Graphene Nanoribbon. *Small* **2013**, *9*, 2405−2409.

(22) Zhang, C.; Peng, Z.; Lin, J.; Zhu, Y.; Ruan, G.; Hwang, C. C.; Lu, W.; Hauge, R. H.; Tour, J. M. Splitting of a Vertical Multiwalled Carbon Nanotube Carpet to a Graphene Nanoribbon Carpet and Its Use in Supercapacitors. *ACS Nano* **2013**, *7*, 5151−5159.

(23) Shelton, J. C.; Patil, H. R.; Blakely, J. M. Equilibrium Segregation of Carbon to a Nickel (111) Surface: A Surface Phase Transition. *Surf. Sci.* **1974**, *43*, 493−520.

(24) Fujita, D.; Yoshihara, K. Surface Precipitation Process of Epitaxially Grown Graphite (0001) Layers on Carbon-doped Nickel (111) Surface. *J. Vac. Sci. Technol., A* **1994**, *12*, 2134.

(25) Sutter, P. W.; Flege, J. I.; Sutter, E. A. Epitaxial Graphene on Ruthenium. *Nat. Mater.* **2008**, *7*, 406−411.

(26) Orofeo, C. M.; Ago, H.; Hu, B.; Tsuji, M. Synthesis of Large Area, Homogeneous, Single Layer Graphene Films by Annealing Amorphous Carbon on Co and Ni. *Nano Res.* **2011**, *4*, 531−540.

(27) Kim, K. S.; Zhao, Y.; Jang, H.; Lee, S. Y.; Kim, J. M.; Kim, K. S.; Ahn, J. H.; Kim, P.; Choi, J. Y.; Hong, B. H. Large-Scale Pattern Growth of Graphene Films for Stretchable Transparent Electrodes. *Nature* **2009**, *457*, 706−710.

(28) Kato, T.; Hatakeyama, R. Site- and Alignment-Controlled Growth of Graphene Nanoribbons from Nickel Nanobars. *Nat. Nanotechnol.* **2012**, *7*, 651−656.

(29) Ferrari, A. C.; Meyer, J. C.; Scardaci, V.; Casiraghi, C.; Lazzeri, M.; Mauri, F.; Piscanec, S.; Jiang, D.; Novoselov, K. S.; Roth, S.; Geim, A. K. Raman Spectrum of Graphene and Graphene Layers. *Phys. Rev. Lett.* **2006**, *97*, 187401.

(30) Malard, L. M.; Pimenta, M. A.; Dresselhaus, G.; Dresselhaus, M. S. Raman Spectroscopy in Graphene. *Phys. Rep.* **2009**, *473*, 51−87.

(31) Graf, D.; Molitor, F.; Ensslin, K.; Stampfer, C.; Jungen, A.; Hierold, C.; Wirtz, L. Spatially Resolved Raman Spectroscopy of Single- and Few-Layer Graphene. *Nano Lett.* **2007**, *7*, 238−242.

(32) Lee, S.; Lee, K.; Zhong, Z. Wafer Scale Homogeneous Bilayer Graphene Films by Chemical Vapor Deposition. *Nano Lett.* **2010**, *10*, 4702−4707.

(33) Lui, C. H.; Li, Z.; Chen, Z.; Klimov, P. V.; Brus, L. E.; Heinz, T. F. Imaging Stacking Order in Few-Layer Graphene. *Nano Lett.* **2011**, *11*, 164−169.

(34) Peng, Z.; Yan, Z.; Sun, Z.; Tour, J. M. Direct Growth of Bilayer Graphene on SiO$_2$ Substrates by Carbon Diffusion through Nickel. *ACS Nano* **2011**, *5*, 8241−8247.

(35) Zhang, Y.; Gomez, L.; Ishikawa, F. N.; Madaria, A.; Ryu, K.; Wang, C.; Badmaev, A.; Zhou, C. Comparison of Graphene Growth on Single-Crystalline and Polycrystalline Ni by Chemical Vapor Deposition. *J. Phys. Chem. Lett.* **2010**, *1*, 3101−3107.

(36) Baraton, L.; He, Z. B.; Lee, C. S.; Cojocaru, C. S.; Chatelet, M.; Maurice, J. L.; Lee, Y. H.; Pribat, D. On the Mechanisms of Precipitation of Graphene on Nickel Thin Films. *EPL* **2011**, *96*, 46003.

(37) Zhu, Y.; Lu, W.; Sun, Z.; Kosynkin, D. V.; Yao, J.; Tour, J. M. High Throughput Preparation of Large Area Transparent Electrodes Using Non-functionalized Graphene Nanoribbons. *Chem. Mater.* **2011**, *23*, 935−939.

(38) Kim, J.; Ishihara, M.; Koga, Y.; Tsugawa, K.; Hasegawa, M.; Iijima, S. Low-Temperature Synthesis of Large-Area Graphene-based Transparent Conductive Films Using Surface Wave Plasma Chemical Vapor Deposition. *Appl. Phys. Lett.* **2011**, *98*, 091502.

(39) Yu, K.; Lu, G.; Bo, Z.; Mao, Z.; Chen, J. Carbon Nanotube with Chemically Bonded Graphene Leaves for Electronic and Optoelectronic Applications. *J. Phys. Chem. Lett.* **2011**, *2*, 1556−1562.

(40) Kis, A.; Csanyi, G.; Salvetat, J. P.; Lee, T. N.; Couteau, E.; Kulik, A. J.; Benoit, W.; Brugger, J.; Forro, L. Reinforcement of Single-walled Carbon Nanotube Bundles by Intertube Bridging. *Nat. Mater.* **2004**, *3*, 153−157.

(41) Nirmalraj, P. N.; Lyons, P. N.; De, S.; Coleman, J. N.; Boland, J. J. Electrical Connectivity in Single-Walled Carbon Nanotube Networks. *Nano Lett.* **2009**, *9*, 3890−3895.

(42) Fu, Y.; Carlberg, B.; Lindahl, N.; Lindvall, N.; Bielecki, J.; Matic, A.; Song, Y.; Hu, Z.; Lai, Z.; Ye, L.; Sun, J.; Zhang, Y.; Zhang, Y.; Liu, J. Templated Growth of Covalently Bonded Three-Dimensional Carbon Nanotube Networks Originated from Graphene. *Adv. Mater.* **2012**, *24*, 1576−1581.

(43) Fowler, R. H.; Nordheim, L. Electron Emission in Intense Electric Fields. *Proc. R. Soc. A* **1928**, *119*, 173−181.

(44) Hunt, C. E.; Glembocki, O. J.; Wang, Y.; Prokes, S. M. Carbon Nanotube Growth for Field-emission Cathodes from Graphite Paste Using Ar-ion Bombardment. *Appl. Phys. Lett.* **2005**, *86*, 163112.

(45) Koh, A. T. T.; Chen, T.; Pan, L.; Sun, Z.; Chua, D. H. C. Effective Hybrid Graphene/Carbon Nanotubes Field Emitters by Electrophoretic Deposition. *J. Appl. Phys.* **2013**, *113*, 174909.

(46) Flexible Field Emission of Nitrogen-Doped Carbon Nanotubes/ Reduced Graphene Hybrid Films. *Small* **2011**, *7*, 95−100.

(47) Schultz, B. J.; Jaye, C.; Lysaght, P. S.; Fischer, D. A.; Prendergast, D.; Banerjee, S. On Chemical Bonding and Electronic Structure of Graphene-Metal Contacts. *Chem. Sci.* **2013**, *4*, 494−502.